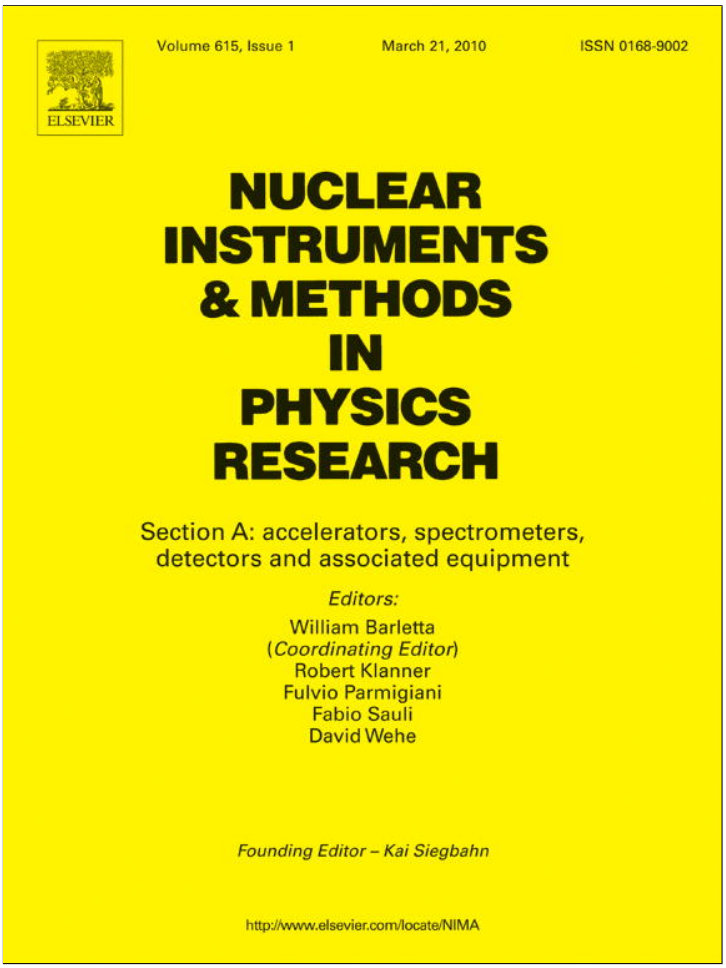

Nuclear Instruments and Methods in Physics Research A 615 (2010) 70–77

Contents lists available at ScienceDirect

Nuclear Instruments and Methods in Physics Research A

journal homepage: www.elsevier.com/locate/nima

Neutron production in a Pb/U-setup irradiated with 0.7–2.5 GeV protons and deuterons

A. Krása [a,*], V. Wagner [a,b], M. Majerle [a], F. Křížek [a], A. Kugler [a], O. Svoboda [a,b], J. Adam [a,c], M.I. Krivopustov [c]

[a] Nuclear Physics Institute ASCR PRI, 250 68 Řež near Prague, the Czech Republic
[b] Faculty of Nuclear Sciences and Physical Engineering, Czech Technical University in Prague, Břehová 7, Prague 1, 115 19, the Czech Republic
[c] Joint Institute for Nuclear Research, Joliot-Curie 6, 141980 Dubna, Russia

ARTICLE INFO

Article history:
Received 26 May 2009
Received in revised form
4 January 2010
Accepted 18 January 2010
Available online 25 January 2010

Keywords:
Spallation
Activation detectors
Threshold reactions
Neutron multiplicity
MCNPX

ABSTRACT

A thick Pb-target with a U-blanket surrounded by a polyethylene moderator was irradiated with 0.7–2.5 GeV proton and deuteron beams. Neutron production was studied with activation detectors. Neutron multiplicity was determined using a modified form of the water-bath/activation-foil method. The experimental results were compared with Monte Carlo simulations performed with the MCNPX code (INCL4+ABLA). Neutron multiplicities on the Pb/U-setup were also compared with data measured on thick Pb-target irradiated with 0.1–4.5 GeV proton beams to date.

1. Introduction

Transmutation of long-lived actinides and fission products from nuclear waste, plutonium from nuclear weapons, or thorium (as an energy source) are being investigated with the increasing interest in the last two decades. Different concepts of transmutation also involve the Accelerator Driven Systems [1] based on a subcritical nuclear reactor driven by an external spallation neutron source.

Spallation is qualitatively well known and has been investigated for many years. However, the spallation applications require more precise knowledge, in particular about emitted neutrons and residual nuclei. The total neutron production (so-called neutron multiplicity), which is of major importance for possible applications, can be predicted for the simplest setup (a bare, thick target) with a precision of 10–15% [2] with any combination of intra-nuclear cascade+evaporation models used in the MCNPX code [3]. General trends of energy, angular or geometry dependence are also well understood, although, local discrepancies, particularly in the 20–80 MeV region, may be as large as a factor of two or so in extreme cases [2,4,5].

"Energy plus Transmutation" (E+T) is an international project [6] that investigates spallation reactions, neutron production and transport, and transmutation of fission products and higher actinides by spallation neutrons [7,8]. The E+T setup (Pb-target/U-blanket) was irradiated with intensive relativistic proton and deuteron beams provided by the Nuclotron accelerator (a superconducting, strong focusing synchrotron) at JINR Dubna, Russia. Spallation neutrons were probed by activation detectors [9–13], solid state nuclear track detectors [13–18], nuclear emulsion techniques [19], He-3 proportional counters [20]. This paper summarizes the neutron production measurements using activation detectors and compares them with Monte Carlo simulations performed with the MCNPX code [3].

2. Experimental apparatus

The E+T setup [6] consists of the three main parts: a cylindrical Pb-target (diameter of 84 mm), a deep-subcritical (k_{eff}=0.202 [21]) ^{nat}U-blanket (hexagonal cross-section with a side length of 130 mm), and granulated $(CH_2)_n$-shielding ($\rho = 0.802\,g\,cm^{-3}$), see Fig. 1. The target/blanket part is 480 mm long and is divided into four sections of 114 mm in length separated by 8 mm gaps, see Fig. 2. Thus, the Pb-target has a length of 456 mm.

The Pb/U-setup is placed in a polyethylene shielding of approximately cubic size ($\approx 1\,m^3$). The inner walls of this container are coated with a Cd-layer with a thickness of 1 mm.

* Corresponding author. Tel.: +420 266 172 652; fax: +420 220 941 130.
E-mail address: krasa@ujf.cas.cz (A. Krása).

0168-9002/$ - see front matter © 2010 Elsevier B.V. All rights reserved.
doi:10.1016/j.nima.2010.01.029

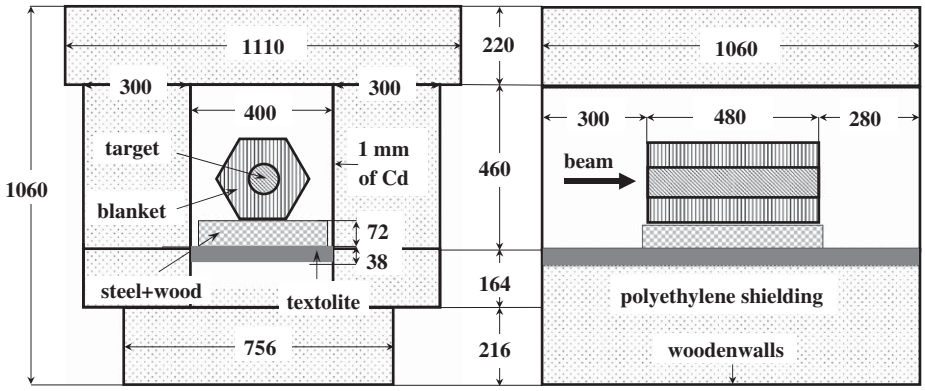

Fig. 1. Front view (left) and cross-sectional side view (right) of the "Energy plus Transmutation" setup. Dimensions are given in millimeters.

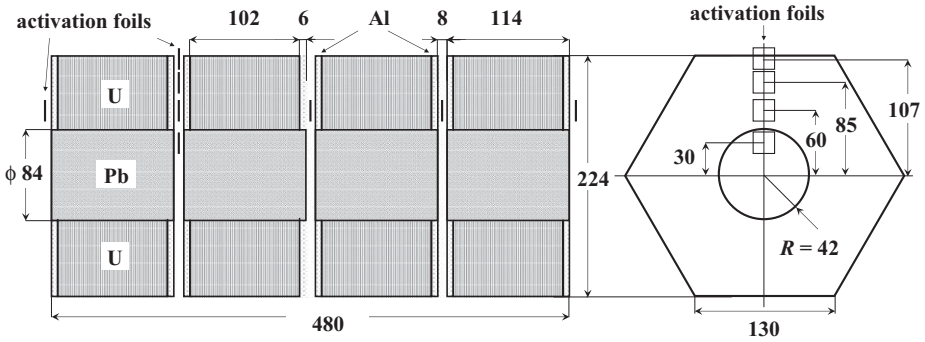

Fig. 2. Typical placement of activation foils: side view (left), cross-sectional view in the first gap (right). Dimensions are given in millimeters.

The front and the back ends of the setup are not shielded. The whole setup mass is 950 kg, thereout the Pb-target weighs 28.6 kg and the U-blanket weighs 206 kg.

Six irradiations of the E+T setup have been performed until now: with proton beams having the kinetic energies of 0.7, 1.0 [22], 1.5 [10], 2.0 GeV and deuteron beams of 0.8 [23], 1.26 [24] A GeV. The detailed analyses of the experiments are described in the references. The integral beam intensities were of the order of $\sim 10^{13}$. The beams had approximately elliptical shape (close to circular) and were parallel to the target axis. Details about the beam monitoring can be found in Refs. [25,26].

The produced neutron field was probed by non-threshold (n,γ)-reaction and threshold (n,α), $(n, x\ n)$-reactions in ^{27}Al-, ^{197}Au-, ^{209}Bi-, ^{59}Co-, ^{nat}In-, ^{181}Ta-foils of an approximate size of $20\times 20\,mm^2$ with a thickness of 0.04–1 mm. Two sets of activation foils were placed in the gaps between target/blanket sections: the first set measured longitudinal distribution and the second set measured radial distribution of the produced neutron field, see Fig. 2.

The activities of the activated foils were measured off-line by lead-shielded HPGe γ−spectrometers. The foils were measured at the distances of 12–311 mm from the detector endcap, which were chosen to achieve the dead time smaller than 10%. The used γ−spectroscopy techniques are described in detail in Ref. [26].

3. Data analysis

The measured γ−spectra were processed by the DEIMOS32 code [27] that provides a Gaussian fit of γ−peaks with energies E. The fitted peak areas $S_\gamma(E)$ were corrected for standard spectroscopic corrections. The final obtained value for each produced isotope is the yield, i.e., the number of activated nuclei per one gram of activated material and per one beam particle:

$$N_{\mathrm{yield}} = \frac{S_\gamma(E)}{m I_{\mathrm{beam}}} \frac{t_{\mathrm{real}}}{t_{\mathrm{live}}} \frac{C_{\mathrm{att}} C_{\mathrm{beam}} C_{\mathrm{decay}} C_{\mathrm{geom}}}{I_\gamma(E)\varepsilon_{\mathrm{p}}(E) C_{\mathrm{coi}}} \tag{1}$$

where m is the activation foil mass, I_{beam} is the total beam flux, t_{real} and t_{live} are real and live times of measurement, $I_\gamma(E)$ is the γ−emission probability, $\varepsilon_{\mathrm{p}}(E)$ is detector efficiency for the measured γ−quanta with the energy E.

C_{coi} is a coincidence correction factor [28] that corrects the yield for the true-coincidence summing and losses effects. C_{coi} varied from 0.8 to 1.3 at closer distances and equaled 1 at larger distances between the foil and the detector.

C_{geom} is a geometrical correction factor accounting for influence of non-zero dimensions of activation foils, whereas, the efficiency calibration was done using point-like calibration sources. C_{geom} was negligible (equal to 1) at larger foil to detector distance, at closer distances reached up to 1.08.

The C_{decay} factor includes corrections for decay from the beginning of the irradiation to the end of the measurement:

$$C_{\mathrm{decay}} = \frac{\exp(\lambda t_{\mathrm{cool}})}{[1-\exp(-\lambda t_{\mathrm{real}})]} \frac{\lambda t_{\mathrm{irr}}}{[1-\exp(-\lambda t_{\mathrm{irr}})]} \tag{2}$$

where t_{cool} is time from the end of the irradiation until the beginning of the measurement, t_{irr} is time of irradiation, $\lambda = \ln 2/T_{1/2}$ is decay constant.

C_{beam} is a correction for beam fluctuations and interruptions during the irradiation:

$$C_{\mathrm{beam}} = \frac{1-\exp(-\lambda t_{\mathrm{irr}})}{t_{\mathrm{irr}} \sum_{i=1}^{N} \left\{ \frac{w(i)}{t_{\mathrm{p}}(i)} \exp(-\lambda t_{\mathrm{e}}(i))[1-\exp(-\lambda t_{\mathrm{p}}(i))] \right\}} \tag{3}$$

where $t_{\mathrm{p}}(i)$ is the duration of i-th interval of irradiation (i.e., a spill), $t_{\mathrm{e}}(i)$ is the time from the end of i-th interval until the end of

the whole irradiation, $w(i)$ is the weight of i-th interval, N is the number of intervals. C_{beam} was important for isotopes with $T_{1/2} \lesssim t_{\mathrm{irr}}$; it went down to 0.8.

C_{att} is a correction for attenuation (self-absorption) of photons, which have to penetrate a thickness x in activated foil:

$$C_{\mathrm{att}} = \frac{\mu(E_\gamma)\varrho x}{1-\exp(-\mu(E_\gamma)\varrho x)} \quad (4)$$

where ϱ is foil density, $\mu(E_\gamma)$ is the total mass attenuation coefficient in units of cm^2/g (values taken from [29]). C_{att} was mostly negligible (equal to 1); for thick foils and at low energies it reached up to 1.14.

4. Yields of activation reactions

4.1. Experimental yields

Products of threshold reactions with E_{thresh} from 5 to 60 MeV (Fig. 5) were measured. The experimental yields of ^{197}Au $(\mathrm{n},x)^{197-x+1}$Au (the emission of up to x=7 neutrons) and ^{27}Al$(\mathrm{n},\alpha)^{24}$Na reactions are presented in the example of the 1 GeV experiment in Fig. 3.

The delineated errors are of statistical origin, given by the errors of the Gaussian fit of γ−peaks. Experimental errors, mainly the inaccuracies of the beam and activation foils displacements, beam intensity, and γ−spectrometer efficiency determinations contribute another 30% [21] as a systematic error, which mainly change the absolute values and to a smaller degree the shape of the observed spatial distribution.

The yields have similar shapes for all observed threshold reactions. The radial distributions of the yields decrease as the intensity of spallation neutron field falls with increasing perpendicular distance from the target (beam) axis, see lower part of Fig. 3.

The longitudinal distributions of the yields change for one order of magnitude and have a maximum in the first gap between the target/blanket sections, see upper part of Fig. 3. The threshold reactions are caused mainly by high-energy spallation neutrons, which have two components: evaporation neutrons emitted isotropically (dominant for $E_{\mathrm{n}} \lesssim 30$ MeV) and cascade neutrons emitted in the forward direction (dominant for bigger neutron energies).

If the primary beam does not change when passing the target, one could expect a maximum of evaporated neutrons around the middle of the target and the maximum of cascade neutrons near to the end of the target. However, the intensity of the primary beam decreases as well as the beam particles interact with the target through nuclear reactions and the beam energy decreases along the target due to the ionisation losses. Therefore, the intensity and energy of the produced spallation neutrons decrease along the target. Consequently, the maximum intensity of the high-energy neutron field is shifted towards the front of the target and the longitudinal distributions of the yields of threshold reactions have a maximum in the first gap between the target/blanket sections. It is possible to see that the yields of reactions with lower threshold (caused mainly by evaporated neutrons) have their maxima a bit closer to the front of the target than the yields of reactions with bigger thresholds (caused mainly by cascade neutrons).

By contrast to threshold reactions, the yields of the non-threshold reaction ^{197}Au$(\mathrm{n},\gamma)^{198}$Au change only slightly, see Fig. 3. The majority of the low-energy neutrons contributing to the (n,γ)-reaction (Fig. 5) are epithermal and resonance neutrons ($0.5\,\mathrm{eV} < E_{\mathrm{n}} < 1\,\mathrm{keV}$) produced by moderation and scattering of spallation neutrons in the polyethylene shielding, see Fig. 4. The produced low-energy neutron field is almost homogenous, decreasing in front of the target and behind it, because the target/blanket assembly is not shielded from its ends, see Fig. 1. This fact is reflected on the yields of ^{198}Au: in the radial direction they are the same and in the longitudinal direction they are slightly lower at both ends.

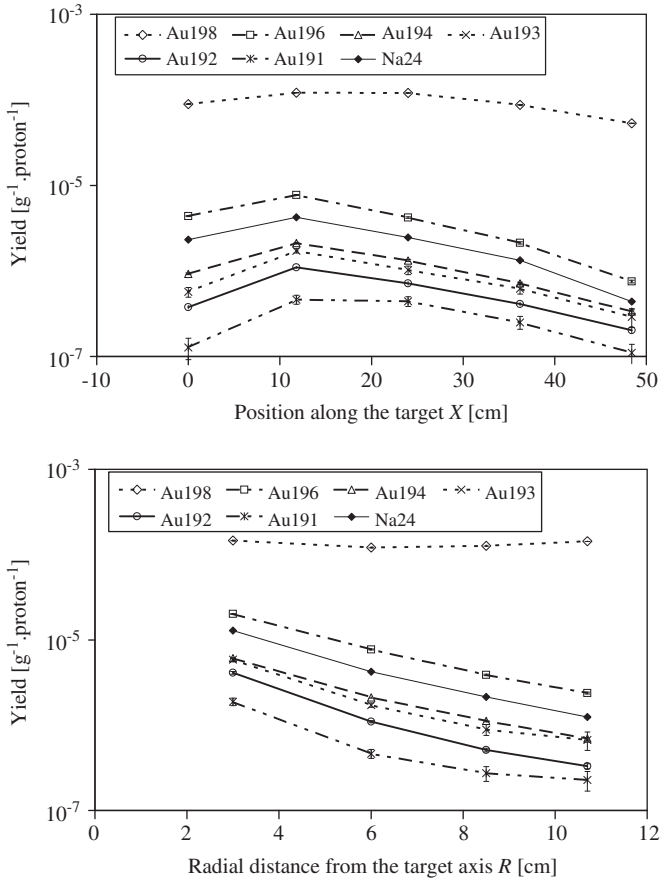

Fig. 3. Longitudinal (top) and radial (bottom) distributions of the experimental yields of nuclei produced in Al- and Au-foils in the 1 GeV experiment. The lines linking experimental points are delineated to guide readers' eyes.

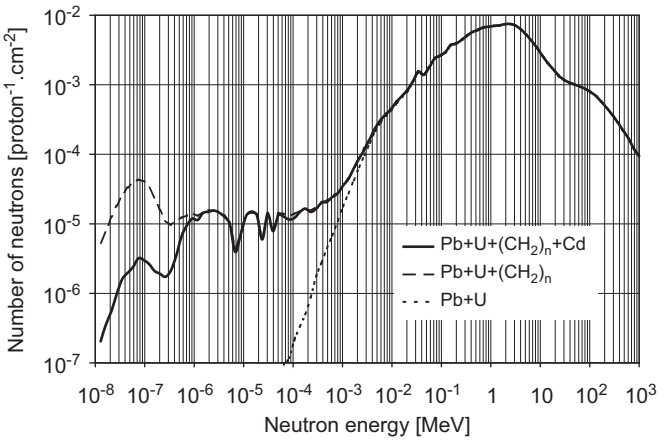

Fig. 4. Influence of the polyethylene shielding and the Cd-layer on the neutron spectra through the first target section. MCNPX simulation of neutron production in the 1 GeV proton irradiation of the E+T setup (Pb+U+Cd+$(CH_2)_n$) and two simplified setups.

4.2. Simulated yields

The Monte Carlo simulations of neutron production in the E+T setup and activation reactions in the foils were performed by the MCNPX code 2.7.A (beta version) [30].

The intra-nuclear cascade (INC) stage of spallation reaction was described using the Liège INC model (so-called INCL4) [33]. INCL4 describes interactions between an impinging particle and target nucleons during intra-nuclear cascade as a sequence of binary collisions separated in space and time. The trajectory between collisions is assumed to be linear. The collisions proceed until a certain degree of equilibrium is reached. The criterion used in INCL4 is an empirical time of equilibrium (so-called cutoff time $t_{cut} \approx 30\,\mathrm{fm/c}$ [34] that allows five sequential nucleon-nucleon interactions on average), which was deduced from a clear change of the calculated quantities (like the integral number of emitted particles, their total kinetic energy or the excitation energy of the residual nucleus). The nuclear density distribution is approximated by a Saxon–Woods density distribution, which is ceased at the radius described with a diffuseness parameter. Fermi motion of the nucleons and the quantum effects of Pauli blocking are taken into account. High-energy parts above the range of INC physics usability are taken from the FLUKA code [35].

INCL4 does not include a pre-equilibrium model and is followed by an equilibrium evaporation that competes with a fission channel. This stage of spallation reaction was described using the ABLA evaporation model (with its built-in fission model) [36]. The LA150 data library [37] was used as the source of the evaluated cross-sections.

Possible inaccuracies in the description of the E+T setup geometry on the produced neutron field are negligible [21]. The influence of individual setup components and experimental conditions on the produced neutron field and the activation yields was also studied [21] using MCNPX. High-energy neutrons (causing threshold reactions) are not influenced by the polyethylene shielding and the Cd-layer, the materials of different holders and other construction details, or by the detectors (no change beyond the statistical uncertainties of simulations which were about 3%).

The low-energy neutron field is strongly influenced by the polyethylene shielding and the Cd-layer. Due to the huge cross-section of the (n,γ) reaction (Fig. 5), self-shielding significantly affects the yields of ^{198}Au. On the other hand, the effect of self-shielding is embodied in simulations as well and no correction for self-shielding was applied to experimental results, see Eq. (1). Self-shielding is negligible for threshold reactions on the foils used, because the respective cross-sections are very small—four orders of magnitude lower than that for neutron capture, see Fig. 5.

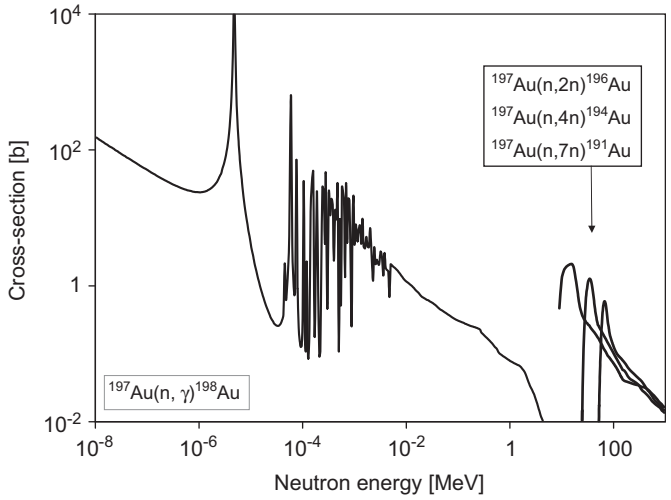

Fig. 5. The cross-section of ^{197}Au(n, γ)^{198}Au from ENDF [31] (left) and the ^{197}Au (n, *x* n)-cross-sections calculated with TALYS ($E_n < 150$ MeV) and MCNPX ($E_n > 150$ MeV) (right).

The simulated yields of ^{198}Au were obtained directly with MCNPX (using the F4 tally with the FM multiplier card) using the ENDF cross-section library [31], see Fig. 5. The comparison between experiment and simulation in the case of non-threshold reaction is discussed in the next section.

The simulations of threshold reactions were done in the three steps: (i) the produced neutron $\Phi_n(E)$ and proton $\Phi_p(E)$ spectra were simulated in the positions of activation foils; (ii) the corresponding cross-sections were calculated using the TALYS code [32] and MCNPX, see Fig. 5; (iii) the yields of threshold reactions were obtained by means of folding of spectra with cross-sections:

$$N_{\mathrm{yield}}(r,z) = \frac{1}{A_r m_u}\int_0^{E_{\mathrm{beam}}} [\Phi_n(E)\sigma_n(E) + \Phi_p(E)\sigma_p(E)]\,\mathrm{d}E \quad (5)$$

where A_r is the specific atomic mass of a chemical element from which the foil was made, m_u is the unified atomic mass unit.

Protons were taken into account as well, because proton-induced reactions (caused mainly by primary protons) leading to the same nuclei as neutron-induced ones (e.g., ^{197}Au(p, pn)^{196}Au) can contribute up to 20% [38,21] to the observed yields. Deuteron caused reactions were also taken into account in the cases where a deuteron beam was used. The influence of other particles (as pions or photons) is negligible in our case (contribution of $< 1\%$) [21].

Typical simulated neutron spectra produced in the E+T setup are presented in Fig. 4. Spallation neutrons overlay the region from 0.1 keV up to the beam energy peaking at about 2 MeV. Clearly observable is the junction between evaporation and cascade part of the neutron spectra around 30 MeV. The low-energy part of the neutron spectra ranging from 10^{-8} MeV up to 1 keV is produced by moderation and scattering of spallation neutrons in the polyethylene shielding. The peak of thermal neutrons (below the cadmium threshold $E_n < 0.5$ eV) is suppressed because of absorbtion in the Cd-layer on the inner walls of the shielding. The oscillations in neutron spectra in the region between 5×10^{-6} and 5×10^{-4} MeV are caused by resonances in the cross-section of neutron capture in ^{238}U that happens in the blanket.

MCNPX describes well the shapes of spatial distributions of yields of threshold reactions, see the example of a relative comparison in Fig. 6. The absolute differences typically reach tens of a per cent, but do not exceed 50% (see an example in Fig. 7). Only in the case of the 1.5 GeV experiment, the ratios between experimental and simulated yields increase considerably with increasing radial distance from the target axis. This trend was observed for all activation foil materials. A similar discrepancy appeared in the case of 2.0 GeV experiment as well, but it is not credible enough due to the missing experimental point at X=11.8, R=3 cm.

It is not clear if the reason for the observed discrepancy comes from the experiment (a possible blunder in data) or the simulation. To solve this problem, a new experiment with the energy 1.5 GeV or bigger is suggested, preferably with a larger set of activation foils located in all gaps between the target/blanket sections. A new experiment could verify the already measured data.

The precision of setup description is on such a level that it cannot be the source of the discrepancy. If the discrepancy originates from the simulation, then the two parts could be

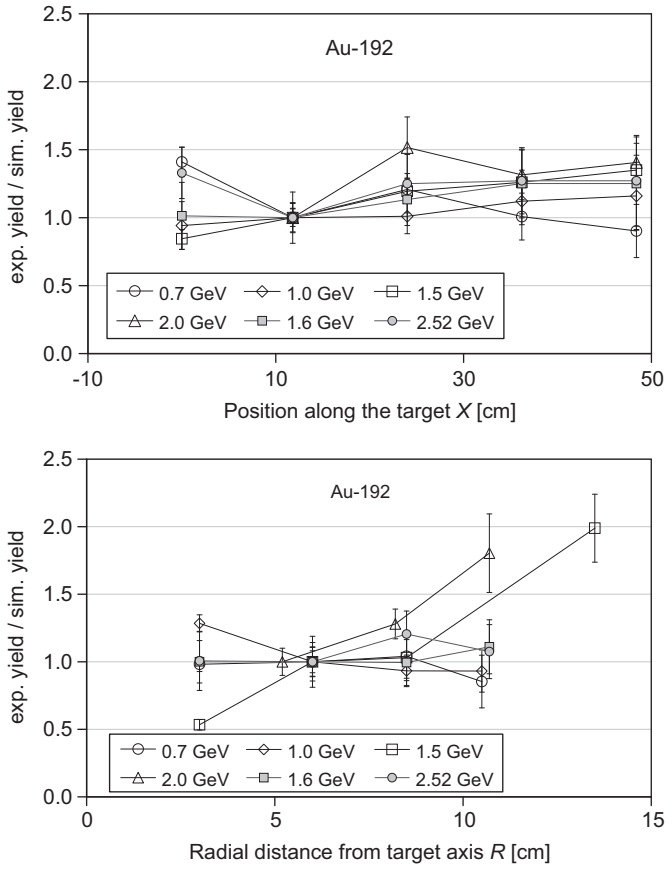

Fig. 6. Relative comparison of experimental and simulated yields of ^{192}Au in longitudinal (top) and radial (bottom) directions for all E+T experiments. Normalized to the second foil in each set.

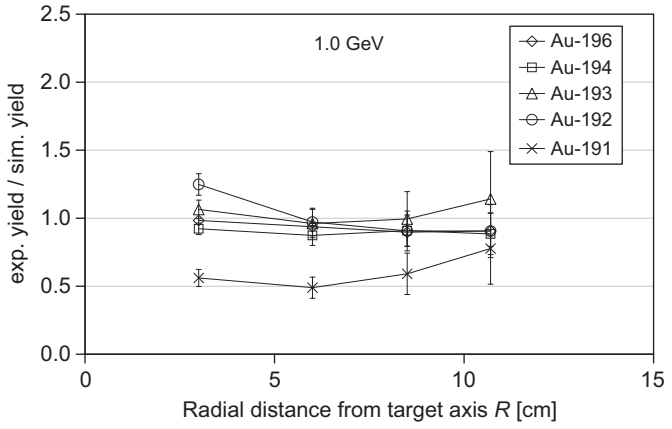

Fig. 7. Absolute comparison of experimental and simulated Au-yields in radial direction for the 1 GeV proton experiment.

responsible for it: the evaluated cross-section libraries or intra-nuclear cascade+evaporation models. The absence of a pre-equilibrium stage might be another reason. It looks like that the angular distribution of the produced high-energy neutrons is not described correctly for beam energies bigger than some value between 1.26 and 1.5 A GeV. A comparison with FLUKA [35] simulations gave similar results [39]. An analogous discrepancy (an underestimation of neutron production for backward angles) was observed on both thick and thin targets [4], however, even for lower beam energies. A fine-tuning of the models could help to reduce the discrepancy between experiment and simulation.

5. Neutron multiplicity

5.1. Neutron multiplicity for Pb-target

The E+T experiments were preceded by an experiment with a simpler setup. The Pb-target (r=4.8, l=50 cm) surrounded by the polyethylene moderator (the same as in the E+T setup) [11,26] was irradiated with a 885 MeV proton beam.

Neutron multiplicity was determined using a modified form of the water-bath/activation-foil method [5] that utilizes a Monte Carlo simulation. The polyethylene acts as a water-bath—it moderates the outgoing neutrons, scatters them back and creates an intensive, homogenous field of low-energy neutrons inside the setup. Its intensity is given by the total number of neutrons leaving the blanket. To measure the intensity of the low-energy neutron field, the ^{197}Au(n,γ)^{198}Au reaction was used. A set of 25 Au-foils was positioned closely above the target. The foils were located side by side all along the target. The production of ^{198}Au, which depends on the total number of neutrons escaping the target, was measured (Fig. 8).

The experimental neutron multiplicity was determined in the following way (according to Ref. [5]). First, the ratio between the experimental and the simulated yields of ^{198}Au was calculated for all used Au-foils. Second, the mean value of these ratios (over all Au-foils) was calculated, see an example in Fig. 11. Then, the experimental neutron multiplicity was obtained by multiplying this mean value and the simulated neutron multiplicity:

$$M_{\mathrm{n}}^{\mathrm{exp}} = M_{\mathrm{n}}^{\mathrm{sim}} \left\langle \frac{N_{\mathrm{yield}}^{\mathrm{exp}}}{N_{\mathrm{yield}}^{\mathrm{sim}}} \right\rangle. \quad (6)$$

This way, the influence of simulations on $M_{\mathrm{n}}^{\mathrm{exp}}$ was suppressed.

The neutron multiplicity on Pb-targets has been studied by a number of experiments. The overview [5] was supplemented with another data extracted from the literature and our own supplementary experiment. The most of the experiments were carried out using a target with a radius of around 5 cm. For this reason all data from different experiments have been rescaled to the case with the radius of 5 cm and the thickness of 100 cm ("saturated thickness" for which a complete saturation of neutron production happens in the considered energy region) by comparing the simulated multiplicities for this "normalized" target size with a real target size. The applied corrections were mostly of the order of a few percent; the only exception are the data [43,50], where the target was very large, resulting in corrections of around 30%.

MCNPX reproduces very well the integral neutron production on a Pb-target in the whole 0.1–4.5 GeV proton energy range, see Fig. 9. Our experimental point is in very good agreement with the

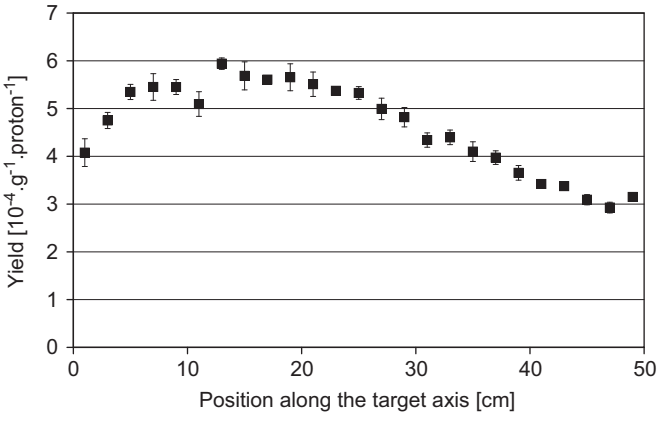

Fig. 8. Longitudinal distribution of the experimental yields of ^{197}Au(n, γ)^{198}Au produced in Au-foils in the p+Pb experiment at 885 MeV.

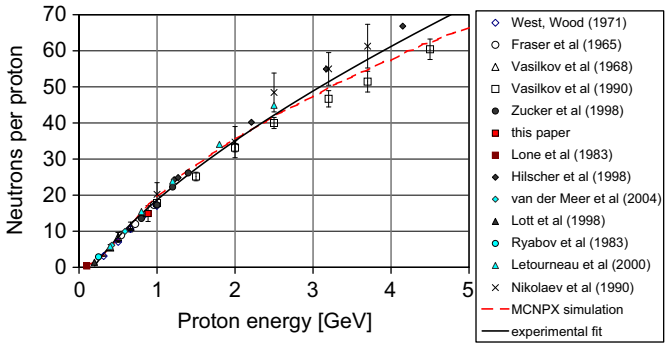

Fig. 9. The compilation of neutron multiplicities for p+Pb have been measured to date. Experimental data were re-counted to the target thickness of 100 cm and the radius of 5 cm and fitted with a power-law function (the solid curve). The dashed curve represents MCNPX simulation. Its statistical uncertainty is ≈0.7%.

others. This is a sign that the method we used for neutron multiplicity determination is applicable in our case, even if water is replaced by a polyethylene moderator that does not fully enclose the target and the foils are located in the aperture between target/blanket and moderator instead of inside the moderator.

The obtained compilation (totally 44 points: West and Wood [41], Fraser et al. [42], Vasilkov et al. [43,40], Zucker et al. [44], our experimental point p+Pb at 885 MeV, Lone et al. [45], Hilscher et al. [46], van der Meer et al. [5], Lott et al. [47], Ryabov et al. [48], Letourneau et al. [49], Nikolaev et al. [50]) was fitted by a power-law function (see Fig. 9):

$$M_n = -8.9 + 27.5E_p^{0.674} \quad (7)$$

where the proton energy E_p is in the units of GeV. This type of empirical formula has been used in earlier papers.

Several authors fitted the energy dependence of neutron multiplicities from proton irradiations of an extended lead target with the radius of 10 cm and the length of 60 cm. Vasilkov et al. [43] presented an empirical formula of a mentioned type based on the experiments with the 1–8.1 GeV protons using the moderation method:

$$M_n = -8.2 + 29.3E_p^{0.75}. \quad (8)$$

Nikolaev et al. [50] presented an empirical formula based on the experiments with the 1–3.7 GeV protons using the method of threshold neutron detectors:

$$M_n = -4.8 + 28.6E_p^{0.85}. \quad (9)$$

Arai et al. [51] presented an empirical formula based on the 12 GeV proton experiment using the Mn-bath moderation method corrected for LAHET simulation and taking into account the results of [50]:

$$M_n = 2.0 + 29.2E_p^{0.78}. \quad (10)$$

Our curve (7) (for r=5 cm, l=100 cm) has a similar shape to the latter mentioned given by the formula (10), see Fig. 10. Neutron multiplicities on the extended target are about 1.5 times bigger than on the "normalized" target.

5.2. Neutron multiplicity for Pb/U-setup

The neutron multiplicities in the E+T experiments were determined using the same method as in the case of 885 MeV proton experiment on the Pb-target. Several Au-foils were added to the standard set of eight Au-foils (Fig. 2) inside the gaps between the target-blanket sections to increase the experimental points, see an example in Fig. 11.

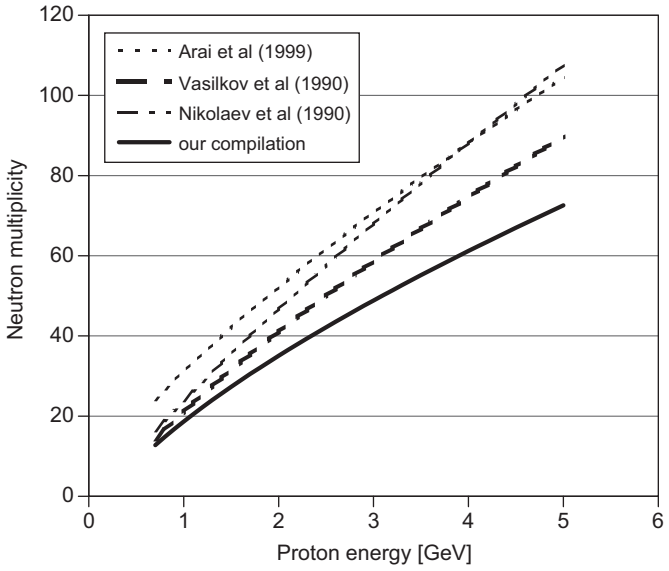

Fig. 10. The comparison of neutron multiplicities for p+Pb. The empirical curves taken from Arai et al. [51], Vasilkov et al. [43], and Nikolaev et al. [50] (all of them for r=10 cm, l=60 cm) are compared with the fit of data compilation in this paper (for r=5 cm, l=100 cm).

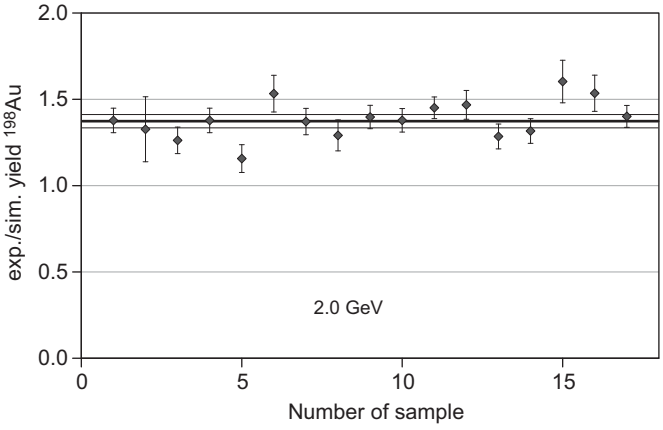

Fig. 11. Ratios between experimental and simulated yields of ^{198}Au for the 2 GeV E+T experiment. Thick solid line represents the weighted average of the ratios, thin solid lines represent its errors.

M_n^{exp} on the E+T setup is 10–40% bigger than M_n^{sim} for all proton and deuteron beams in the 0.7–2.5 GeV range, see Fig. 12. The values of M_n^{exp} agree within the error bars with the neutron multiplicities determined by an integration of the measured neutron flux distribution over the blanket surface [13], see Table 1. The influence of the polyethylene shielding on M_n^{sim} is negligible—the simulations show that the contribution of the neutrons produced in fission in the U-blanket caused by moderated (and back-scattered) neutrons is at the level of 1%.

MCNPX simulations shows that neutron multiplicity on the E+T setup is bigger for deuteron experiments than for proton ones. This tendency grows with the beam energy and reaches 5–20% in the 0.5–3.0 GeV region, see Fig. 13. MCNPX simulations also show that neutron multiplicity is significantly bigger on the E+T setup than that on the Pb-target of the same dimensions as the E+T target. The difference reaches 50–120% in the 0.5–3.0 GeV proton energy region, see Fig. 13. This represents the amount of neutrons gained due to the U-blanket.

As an illustration, the ratios of experimental neutron multiplicities for experiments with similar energies are also plotted in

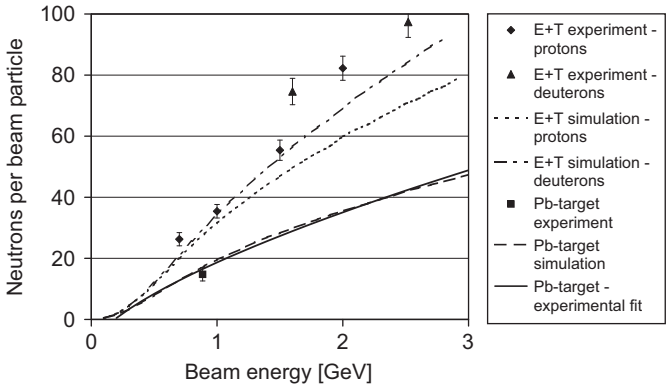

Fig. 12. Compilation of E+T neutron multiplicities compared with MCNPX simulations and the Pb-target (r=5 cm, l=100 cm) experiments.

Table 1
Mean values of ratios between experimental and simulated yields of ^{198}Au, experimental and simulated neutron multiplicities and data by Stoulos et al. [13] for our experiments with the polyethylene moderator. The errors in the third column are errors of the mean value including χ^2. The errors in the fourth column include also errors of the beam integral determination.

Experiment	E_{beam} [GeV]	$\left\langle \frac{N_{yield}^{exp}}{N_{yield}^{sim}} \right\rangle$	M_n^{exp}	M_n^{sim}	M_n^{exp} [13]
p+Pb	0.885	0.87(5)	14.8(2.2)	17.0	–
p+Pb/U	0.7	1.32(4)	26.3(2.2)	20.0	27(2)
	1.0	1.12(4)	35.4(3.3)	31.6	39(3)
	1.5	1.18(5)	55.4(3.3)	46.8	62(5)
	2.0	1.37(3)	82.3(3.9)	59.9	82(6)
d+Pb/U	1.6	1.32(6)	75(9)	56.6	–
	2.52	1.16(3)	97(10)	84.3	–

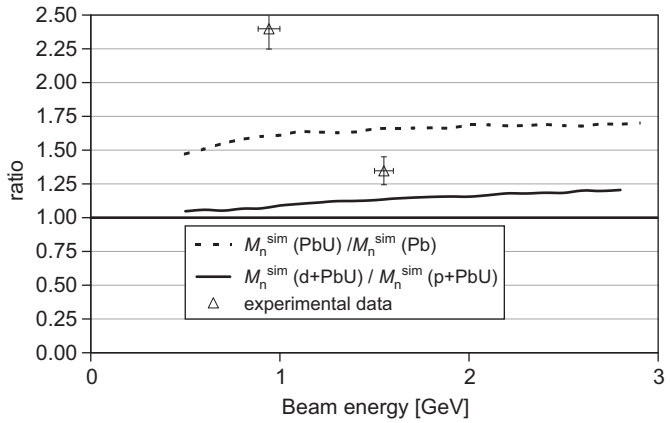

Fig. 13. Ratios of simulated neutron multiplicities for: the deuteron experiments with the E+T setup versus the proton ones; the E+T setup versus the Pb-target of the same dimensions as the the E+T target (r=4.2 cm, l=45.6 cm). As an illustration, ratios of experimental neutron multiplicities for experiments with similar energies are also plotted: PbU (1 GeV)/Pb (0.885 GeV) and d+PbU (1.6 GeV)/p+PbU (1.5 GeV).

Fig. 13: PbU (1 GeV)/Pb (0.885 GeV) and d+PbU (1.6 GeV)/p+PbU (1.5 GeV). The differences between experimental and simulated ratios are much bigger than the experimental errors. The reason is that whereas M_n^{exp} is bigger than M_n^{sim} in the case of the PbU-setup, it is vice versa in the case of the Pb-target. This is strengthened by the fact that M_n increases much more steeply with the beam energy in the case of the PbU-setup than the Pb-target. That is why the difference between M_n (1 GeV) and M_n (0.885 GeV) is much bigger for the PbU-setup than for Pb-target.

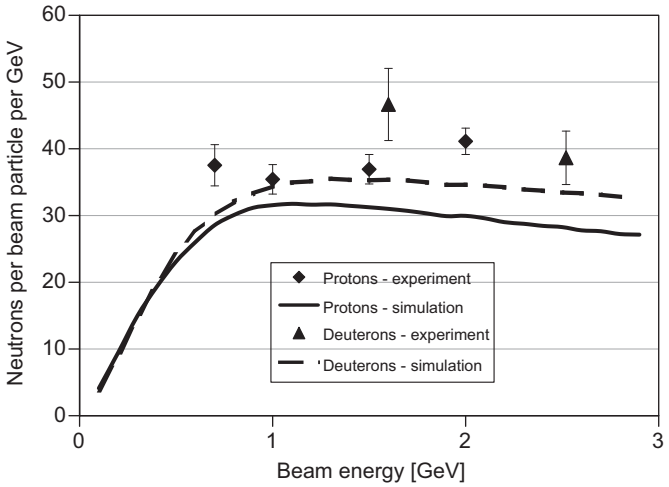

Fig. 14. Dependence of neutron cost on beam energy. Experimental data of the E+T proton and deuteron experiments compared with MCNPX simulations.

While, the integral neutron production (multiplicity) on the E+T setup increases with the beam energy in the 0.7–2.5 GeV range, it saturates around 1 GeV when normalized per unit of beam energy (so-called neutron cost), see Fig. 14. Hence, the optimal beam energy for neutron production appears to be around this value, which agrees with results regarding Pb-target [52]. While the saturation is clearly visible from simulations, experimental neutron cost almost does not change in 0.7–2.5 GeV region and due to big uncertainties of experimental data it cannot be drawn from the performed experiments where the saturation begins.

6. Conclusion

Relativistic proton and deuteron beams were used to irradiate the thick, lead target with the uranium blanket surrounded by the polyethylene moderator. The produced neutron field was studied with activation detectors and compared with MCNPX simulations. The maximum intensity of the high-energy neutron field produced in the Pb/U-assembly was located in the region between the first and second target/blanket sections.

Epithermal and resonance neutrons were produced mainly by moderation (and back-scattering) in the polyethylene shielding. This homogenous low-energy neutron field was used for neutron multiplicity determination, which was found to be larger than the simulated one (but for $<40\%$). For simpler setup, such as Pb-target, MCNPX describes the integral neutron production with the accuracy better than 10% in the 0.1–4.5 GeV proton energy range. Adding the U-blanket can considerably increase the neutron multiplicity. The difference between neutron multiplicities on the Pb/U-setup is slightly favourable for the deuteron experiments compared to the proton ones. This is more distinctive for higher beam energies.

MCNPX describes well the shapes of yields of neutron threshold reactions in the Pb/U-setup. The only exceptions are the 1.5 and 2.0 GeV proton experiments, where the simulations predict steeper decrease of the yields with growing radial distance than what was measured. From the obtained experimental data it is impossible to conclude whether the disagreement is caused by the cascade+evaporation models not tuned for higher beam energies, or it is the experimental error. A new experiment at the energy 1.5 GeV or higher is proposed to verify the experimental data.

Acknowledgments

The authors thank LHE JINR Dubna, especially Prof. A.D. Kovalenko, for providing the Nuclotron accelerator for the irradiations of the E+T setup. This work was carried out with the support of the GA CR (Grant no. 202/03/H043) and GA AS CR (Grant no. K2067107).

References

[1] H. Nifenecker, et al., Prog. Part. Nucl. Phys. 43 (1999) 683.
[2] S. Leray, et al., Nucl. Instr. and Meth. A 562 (2006) 806.
[3] D.B. Pelowitz, et al., LANL Report LA-CP-07-1473, 2008.
[4] S. Meigo, et al., Nucl. Instr. and Meth. A 431 (1999) 521.
[5] K. van der Meer, et al., Nucl. Instr. and Meth. B 217 (2004) 202.
[6] M.I. Krivopustov, et al., Kerntechnik 68 (2003) 48;
M.I. Krivopustov, et al., JINR Dubna Preprint P1-2000-168.
[7] J. Adam, et al., PRAMANA J. Phys. 68 (2007) 297;
J. Adam, et al., JINR Dubna Preprint E15-2008-118.
[8] M.I. Krivopustov, et al., JINR Dubna Preprint E1-2004-79.
[9] M. Majerle, et al., Nucl. Instr. and Meth. A 580 (2007) 110.
[10] F. Křížek, et al., Czechoslov. J. Phys. 56 (2006) 243.
[11] A. Krása, et al., AIP Conf. Proc. 769 (2005) 1555.
[12] A. Krása, et al., J. Phys. Conf. Ser. 41 (2006) 306.
[13] S. Stoulos, et al., Nucl. Instr. and Meth. A 599 (2009) 106.
[14] S.R. Hashemi-Nezhad, et al., Nucl. Instr. and Meth. A 591 (2008) 517.
[15] S.R. Hashemi-Nezhad, et al., Radiat. Meas. 43 (2008) S204.
[16] M. Zamani, et al., Radiat. Meas. 43 (2008) S151.
[17] M. Fragopoulou, et al., Radiat. Prot. Dosim. 132 (2008) 277.
[18] M. Zamani, et al., Nucl. Instr. and Meth. A 508 (2003) 454.
[19] D. Chultem, et al., JINR Dubna Preprint P1-2003-59.
[20] M. Manolopoulou, et al., Nucl. Instr. and Meth. A 562 (2006) 371.
[21] M. Majerle, et al., JINR Dubna Preprint E15-2007-82.
[22] A. Krása, et al., JINR Dubna Preprint E15-2007-81.
[23] M.I. Krivopustov, et al., JINR Dubna Preprint E1-2008-54.
[24] M.I. Krivopustov, et al., J. Radioanal. Nucl. Chem. 279 (2009) 567;
M.I. Krivopustov, et al., JINR Dubna Preprint E1-2007-7.
[25] I.V. Zhuk, et al., Radiat. Meas. 43 (2008) S210.
[26] A. Krása, et al., JINR Dubna Preprint E1-2005-46.
[27] J. Frána, J. Radioanal. Nucl. Chem. 257 (2003) 583.
[28] F. De Corte, The k0-standardization method. A move to the optimization of neutron activation analysis, Ryksuniversiteit Gent: Facultei Van de Wetenschappen, 1986.
[29] J.H. Hubbell, S.M. Seltzer, Tables of X-Ray Mass Attenuation Coefficients and Mass Energy-Absorption Coefficients, National Institute of Standards and Technology, Gaithersburg, MD, 2004 〈http://physics.nist.gov/xaamdi〉.
[30] D.B. Pelowitz, et al., LANL Report LA-UR-08-07182, 2008.
[31] 〈http://www.nndc.bnl.gov/exfor/endf00.htm〉.
[32] A.J. Koning, S. Hilaire, M.C. Duijvestijn, AIP Conf. Proc. 769 (2005) 1154.
[33] A. Boudard, et al., Phys. Rev. C 66 (2002) 044615.
[34] L. Pienkowski, et al., Phys. Lett. B 336 (1994) 147.
[35] A. Fasso, et al., CERN-2005-10 (2005), INFN/TC 05/11, SLAC-R-773.
[36] A.R. Junghans, et al., Nucl. Phys. A 629 (1998) 635.
[37] M.B. Chadwick, et al., Nucl. Sci. Eng. 131 (1999) 293.
[38] A. Krása, et al., in: Proceedings of the International Workshop on Nuclear Data for Transmutation Nuclear Waste, GSI-Darmstadt, Germany, 1–5 September 2003, ISBN 3-00-012276-1.
[39] M. Oden, et al., AIP Conf. Proc. 958 (2007) 219.
[40] R.G. Vasilkov, et al., At. Energiya 25 (1968) 479.
[41] D. West, E. Wood, Can. J. Phys. 49 (1971) 2061.
[42] J.S. Fraser, et al., Phys. Canada 21 (1965) 17;
J.S. Fraser, et al., in: Proceedings of the Annual Meeting of the Canadian Association of Physics, Vancouver, 10 June 1965.
[43] R.G. Vasilkov, V.I. Yurevich, in: Proceedings of the 11th Meeting of International Collaboration on Advanced Neutron Sources ICANS-11 KEK, Tsukuba, Japan, 22–26 October 1990, KEK Report 90-25, vol. 1, 1991, p. 340.
[44] M.S. Zucker, et al., Nucl. Sci. Eng. 129 (1998) 180.
[45] M.A. Lone, et al., Nucl. Instr. and Meth. 214 (1983) 333.
[46] D. Hilscher, et al., Nucl. Instr. and Meth. A 414 (1998) 100.
[47] B. Lott, et al., Nucl. Instr. and Meth. A 414 (1998) 117.
[48] Yu.V. Ryabov, G.K. Matushko, V.N. Slastnikov, Zeitschr. Phys. A 311 (1983) 363.
[49] A. Letourneau, et al., Nucl. Instr. and Meth. B 170 (2000) 299.
[50] V.A. Nikolaev, et al., in: Proceedings of the 11th Meeting of International Collaboration on Advanced Neutron Sources ICANS-11 KEK, Tsukuba, Japan, 22–26 October 1990, KEK Report 90-25, vol. 1, 1991, p. 612.
[51] M. Arai, et al., J. Neutron Res. 8 (1999) 71.
[52] A.V. Dementyev, N.M. Sobolevsky, Yu.Ya. Stavissky, Nucl. Instr. and Meth. A 374 (1996) 70.